Electric Power Systems Research 193 (2021) 107013

Contents lists available at ScienceDirect

Electric Power Systems Research

journal homepage: www.elsevier.com/locate/epsr

Partial discharge location of power cables based on an improved single-terminal method

Rui Liang [a], Zhe Zhang [a], Hailong Li [b], Peng Chi [a], Guoxin Li [a,*], Yunchun Tao [a]

[a] School of Electrical and Power Engineering, China University of Mining and Technology, Xuzhou, 221116, China
[b] State Grid Sanmenxia Power Supply Company, Henan 472099, China

ARTICLE INFO

Keywords:
Partial discharge (PD)
PD location
Power cable
Parameterless adaptive threshold empirical wavelet transform
Single-terminal method

ABSTRACT

The precise location of partial discharge (PD) in power cables is of great significance to ensure the stable operation of the power grid. Therefore, aiming at the problem of the PD location accuracy is the affected by the uncertainty of the wave velocity, an improved single-terminal method is used to estimate the PD location of power cables. In the proposed method, the wave velocity and arrival time difference of the PD signal are modified, so that it has a higher location accuracy and better robustness. Meanwhile, in order to improve the location accuracy of the PD location method in a noisy environment, the denoising algorithm of parameterless adaptive threshold empirical wavelet transform (PATEWT) is proposed in the paper. Compared with the traditional single-terminal method and two-terminal method, the proposed algorithm has a good denoising performance. Finally, simulations are provided to verify the effectiveness and feasibility of the proposed method.

1. Introduction

With the increasing demand of the power, there is no doubt that the high voltage power cables have played a very important role in power transmission. Due to the environmental, mechanical and electrical factors, the insulation aging process of the power cable is accelerated, which increases the occurrence of faults. Therefore, we need to detect the partial discharge (PD) signals and locate the PD power sources in the initial stage of power cable aging, so that it can exclude the fault in advance and prevent breakdown accidents [1-3].

When the various equipment in the power system operate together, it may cause the detected PD signal to contains plenty of noise information, which reduces the reliability of the PD signal and affects the judging result [4]. Therefore, before positioning the PD signal, it is necessary to adopt an effective denoising method to suppress the noise signal, thus the location accuracy is improved.

In order to further denoise the PD signals, many methods have been proposed to estimate the location accuracy of the PD sources. For instance, the discrete wavelet transform and the wavelet transform technology are utilized in [5] and [6], respectively. However, there are several problems when the two methods are applied to PD signal denoising. For example, due to the diversity of PD signals, it is difficult to choose a wavelet basis function that is completely suitable for the PD pulse waveform, and the decomposition scale is also not unique. In order to solve the problems of decomposition scale, the Empirical mode decomposition (EMD) is adopted, but it has the difficulty in selecting a fixed threshold. To effectively address these challenges, Singular value decomposition technology (SVD) is used in [7] to implement the denoising process of the PD signals. However, it loses the processed signal partially because of the unchanged singular value. Then, an adaptive singular value decomposition (ASVD) method in [8] is proposed, but it has the problem of selecting a threshold value.

In addition, Time-domain reflectometry (TDR) is one of the PD location methods commonly used in recent years [9-11]. This method estimates the PD location by using the time difference acquired from the first pulse signal measured by the sensor and the pulse signal reflected from the opposite terminal. It has a high accuracy, but the propagation velocity and the length of the cable must be pre-known. Meanwhile, the partial discharge signal has dispersion and attenuation problems in the process of propagation when the method is applied to long-distance cables [12-13]. Therefore, the single-terminal location method using TDR is suitable for PD location for short-distance cables. At the same time, even though the two-terminal location method using TDR overcomes the defects of single-terminal detecting and is suitable for PD location of long-distance cables, the location accuracy is restricted by the synchronization of two-terminal time system. Since the wave

* Corresponding author.
E-mail address: lgx@cumt.edu.cn (G. Li).

https://doi.org/10.1016/j.epsr.2020.107013
Received 5 August 2020; Received in revised form 25 November 2020; Accepted 22 December 2020
Available online 6 January 2021

velocity will change with the distance when the PD signal propagates in power cables, so that the accuracy of the PD source will be affected if a fixed wave velocity is used [14]. In [15], the phase difference between the incident wave and the reflected wave in the frequency domain is analyzed to achieve the location of PD signals, and the arrival time of the PD signal is not required. However, the location accuracy will be affected because of the fixed wave velocity as well. In [16], the frequency-dependent characteristic of the phase velocity is considered and the phase velocity is used to modify the phase difference of the PD signal. However, its location accuracy may also be affected by the sampling rate, the quantization error and the length of cable.

In view of the above problems, this paper proposes a novel PD location method that combines the denoising algorithm of parameterless adaptive threshold based on empirical wavelet transform (PATEWT) and PD location method of power cables based on improved single-terminal method. Firstly, the empirical wavelet transform (EWT) is used to decompose the PD signal and the Fourier spectrum is divided automatically by scale space method. Then it uses an adaptive threshold function for threshold processing, thus the denoising of the PD signal is implemented. Moreover, the arrival time of the PD signal is determined by S-transform, and the measured data is substituted into the improved single-terminal method to calculate the defect position of the PD sources. Finally, it can be verified by the simulation that the novel method has a high location accuracy compared with different signal-to-noise ratios (SNR) and PD sources at different positions.

The reminder of this paper is organized as follows. Section 2 depicts the process of the denoising algorithm, including EWT, parameterless space-scale method, and construction of the adaptive threshold function. In Section 3, the principle of cable PD location method and the location procedure of improved single-terminal method are presented in details. In Section 4, the experimental simulation is performed on the PSCAD software to verify the feasibility and effectiveness of the proposed method. Finally, the conclusions are drawn in Section 5.

2. PD signal denoising methods

2.1. Empirical wavelet transform

The empirical wavelet transform (EWT) is based on empirical mode decomposition and wavelet analysis and it has a complete theoretical system of wavelet analysis. The calculation complexity is much smaller than empirical mode decomposition. Moreover, it solves the problem of modal aliasing which existed in the empirical mode decomposition, so the robustness of the algorithm is improved and the applicability of the algorithm is expanded [17]. The procedure of EWT can be shown as follows:

Firstly, the Fourier transform is performed in the original signal $f(t)$, and the spectrum is divided accordingly. Then, the modal number is denoted as N and the frequency range of $f(t)$ is $[0, \pi]$, according to the local minima found in spectrum, we can sort them by amplitude from largest to smallest. Finally, the spectrum is divided into N parts by taking the first N-1 of the local minima as the boundary lines. The intermediate frequency between two continuous local maxima is defined as the boundary ω_n of each continuous spectrum.

Then, the wavelet filter bank is constructed. When the division of frequency bands is determined, the appropriate empirical wavelet scale function $\widehat{\Psi}_n(\omega)$ and wavelet function $\widehat{\varphi}_n(\omega)$ are constructed by using Meyer wavelet. Empirical wavelet scale function $\widehat{\Psi}_n(\omega)$ and wavelet function $\widehat{\varphi}_n(\omega)$ can be expressed as:

$$\widehat{\Psi}_n(\omega)=\begin{cases}1,(1+r)\omega_n\le|\omega|<(1-r)\omega_{n+1}\\ \cos\left[\frac{\pi}{2}\beta\left(\frac{1}{2r\omega_{n+1}}(|\omega|-(1-r)\omega_{n+1})\right)\right],(1-r)\omega_{n+1}\le|\omega|<(1+r)\omega_{n+1}\\ \sin\left[\frac{\pi}{2}\beta\left(\frac{1}{2r\omega_n}(|\omega|-(1-r)\omega_n)\right)\right],(1-r)\omega_n\le|\omega|<(1+r)\omega_n\\ 0,others\end{cases} \tag{1}$$

$$\widehat{\varphi}_n(\omega)=\begin{cases}0,|\omega|<(1-r)\omega_n\\ \cos\left[\frac{\pi}{2}\beta\left(\frac{1}{2r\omega_n}(|\omega|-(1-r)\omega_n)\right)\right],(1-r)\omega_n\le|\omega|<(1+r)\omega_n\\ 1,others\end{cases} \tag{2}$$

where

$$\beta(x)=x^4\left(35-84x+70x^2-20x^3\right) \tag{3}$$

$$r<\min_n\left(\frac{\omega_{n+1}-\omega_n}{\omega_{n+1}+\omega_n}\right) \tag{4}$$

Lastly, the time domain signals of each mode are obtained. The detail coefficients of the empirical wavelet transform are obtained from the wavelet filter bank, then the original signal is reconstructed according to the detail coefficients. In this way, the time domain signal of each mode is gained.

2.2. Parameterless scale-space method

The reasonable division of the Fourier spectrum is of great importance in EWT. The common method used in EWT needs to determine the modal number N in view of experience [18], but due to the spectrum range of PD signal is comparatively large, the SNR differs greatly when different modes number N are selected. Therefore, in this paper, the scale-space method is introduced to automatically divide the Fourier spectrum. The corresponding information can be obtained by constantly changing the scale parameters, so that the original signal can achieve adaptive and parameterless decomposition.

$L(X, t)$ is a function of x. The number of initial partial minimum point is denoted by n and each of initial partial minimum is defined as a "scale-space curve" C_i of length $L_i (i \in [1, n])$. If the local minima which is consistent with the relative scale parameter t is defined as the boundary, it is equivalent to find a threshold T, so that the scale-space curves of length larger than T are the curves corresponding to the consistent minima. That is, the scale-space curve of length larger than T is the division curve of the Fourier spectrum as well [19]. In this paper, the empirical distribution is adopted to determine the threshold T.

Given a positive small number ε, the i th initial partial minimum point can be denoted as:

$$P(L_i>T)\le\varepsilon \tag{5}$$

where the expression of T is different under the different distribution law P. For example, if P is the empirical distribution, it has:

$$\sum_{k=1}^{T}H_L(k)=(1-\varepsilon)\sum_{k=1}^{T}H_L(k) \tag{6}$$

where H_L represents the occurrences of the length of the scale-space curve.

2.3. Adaptive threshold function

The selection of threshold functions is essential to the denoising of noisy signals. Traditional methods mainly include hard and soft threshold function [20], and the expressions of the hard and the soft threshold function are defined as follows:

$$\hat{f}(t) = \begin{cases} f(t) & |f(t)| \geq \lambda \\ 0 & |f(t)| < \lambda \end{cases} \quad (7)$$

$$\hat{f}(t) = \begin{cases} \mathrm{sgn}(f(t))(|f(t)| - \lambda) & |f(t)| \geq \lambda \\ 0 & |f(t)| < \lambda \end{cases} \quad (8)$$

where *f*(*t*) represents the noisy signal. $\lambda = \sigma\sqrt{2\ln(\mathrm{N})}$ represents the value of the threshold. σ is the estimation of the standard deviation and *N* is the length of the noisy signal *f*(*t*).

In order to further improve the denoising effect, this paper proposes a new adaptive threshold function combining the hard and the soft threshold function, the expression can be presented as follows:

$$\hat{f}(t) = \begin{cases} \mathrm{sgn}(f(t))\left(|f(t)| - \dfrac{1.2\lambda}{e^{|f(t)|-\lambda}}\right) & |f(t)| \geq \lambda \\ 0 & |f(t)| < \lambda \end{cases} \quad (9)$$

The comparison of the adaptive threshold function,the soft and hard threshold function in the same coordinate system is shown in Fig. 1. It can be seen from Fig. 1 that the f(t) processed by the hard-threshold function is discontinuous at λ, which causes new oscillations in the de-noised signal. The soft-threshold function is continuous at λ, but there is a fixed difference between the de-noised f(t) and the original f(t), which makes the denoised signal produce certain distortion. The adaptive threshold function proposed in this paper is continuous at λ, which overcomes the discontinuity of hard threshold function. Meanwhile, when f(t) increases gradually, it can approximate f(t) quickly and overcome the problem of fixed difference in soft-threshold function.

2.4. PATEWT denoising algorithm

The denoising procedure of proposed PATEWT algorithm is as follows:

Firstly, the original signal is decomposed by EWT, i.e., the Fourier spectrum is divided by using the scale-space method and the reasonable orthogonal wavelet filter group is obtained. So the amplitude modulation (AM) and the frequency modulation (FM) sub-signals can be gained, in which the Hilbert transform is further adopted to get the signal components of multiple frequencies.

Then, wavelet threshold denoising is performed on each signal component where the threshold function adopts the proposed adaptive threshold function.

Lastly, Signal reconstruction is performed based on EWT to achieve original signal denoising.

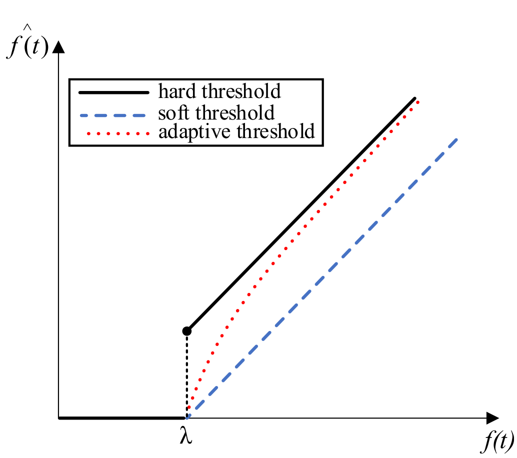

Fig. 1. Waveform comparison of adaptive threshold function and soft and hard threshold function.

3. PD location method

3.1. S transform

In this paper, the PD signal propagated in cables is analyzed by S transform and then the arrival time of the PD signal is collected. S transform is a time-frequency analysis algorithm by combining the Fourier transform and wavelet transform [21], which is reversible. Compared with wavelet transform, the S transform overcomes the defect of the short-time Fourier transform which the window is fixed, thus, the window function of the S transform can be flexibly adjusted on the time axis, and the frequency function will also change accordingly.

S transform can be expressed as:

$$S(t,f) = \int_{-\infty}^{+\infty} w(t-\tau,f)x(\tau)e^{-2j\pi f\tau}dt \quad (10)$$

Where *x*(*t*) is the time domain signal, *w*(*t*-*τ*) is the window function, *τ* is the time offset factor, and *f* is the frequency.

The Gaussian function can be expressed as:

$$w(t-\tau,f) = \frac{1}{\sigma\sqrt{2\pi}}e^{\frac{-(t-\tau)^2}{2\sigma^2}} \quad (11)$$

Where *σ* is the width of the window function.

$$\sigma = \frac{1}{|f|} \quad (12)$$

As shown in Eqs. (10)–(12), in S-transform, when the frequency of non-stationary signals becomes lower, the width of the window function will be larger, and the frequency resolution will be correspondingly higher. On the contrary, when the frequency of non-stationary signals becomes higher, the width of the window function will be smaller, and the time resolution will be higher.

3.2. Traditional single-terminal location method

Fig. 2 shows the principle of the traditional single-terminal location method. The total length of the cable is *L* and its two ends are denoted by A and B respectively. As illustrated in Fig. 2, the PD pulse generated from the position of cable insulation defect at time T_0. The distance between PD location and end A is L_A and that between end B is L_B, satisfying $L_A + L_B = L$. In this way, the PD pulse starts to travel towards end A with length L_A at time t_{a1}, and the distance L_A satisfies the following condition:

$$L_A = v_0(t_{a1} - T_0) \quad (13)$$

Where v_0 is the actual propagation velocity of the PD signal in the cable. Meanwhile, another PD pulse is reflected from end B at a distance L_B from defect position and reaches end A through the total length *L* at time t_{a2}. Thus, the following conditions are satisfied [22]:

$$L_B + L = v_0(t_{a2} - T_0) \quad (14)$$

$$L_A + L_B = L \quad (15)$$

According to Eqs. (13),–(15), the distance L_A can be derived as:

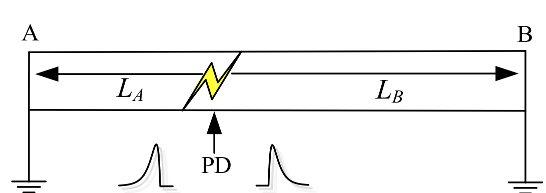

Fig. 2. Single-terminal location method for PD of power cables.

$$L_A = L - \frac{1}{2}v_0(t_{a2} - t_{a1}) \tag{16}$$

In addition, the length of cable L and the propagation velocity v_0 are required if the single-terminal location method is used. Although the length of the cable can be measured, the propagation velocity is difficult to gain an accurate value, which may increase the error of the measurement results. In the information of two arrival time of the PD pulses measured at end A, it has different propagation distance and propagation velocity, which may result in the deviation of the results as well.

3.3. PD location of power cables based on improver single-terminal method

The wave velocity is not fixed when the PD pulse is propagated in the cables, it will change with the change of propagation distance, which means it will produce location error if the fixed empirical propagation velocity is adopted. Therefore, the value of wave velocity cannot be the same [14]. Based on traditional single-terminal location method, this paper considers the uncertainty of wave velocity and makes further improvements.

As shown in Fig. 3, in the proposed location method, the traditional single-terminal method is adopted at both ends to detect the PD pulses, so the PD pulses are collected at end A and end B. The PD monitoring system consists of sensors, digital-to-analog converters and personal computers. Therefore, if the empirical estimation propagation velocity v is used as the initial value of the wave velocity before substituting it into the improved single-terminal method, it may result in an error in location result due to the deviation from the actual value. The calculated location results are denoted by X_A, X_B which means there exists an error between calculation values X_A, X_B, and the actual values L_A, L_B.

In view of the above analysis, when the pulses are measured at end A, the arrival time of the PD pulses can be obtained based on S transform. The first arrival time and the second arrival time of the PD pulses toward end A are denoted by t_{a1} and t_{a2}, respectively. Similarly, when the pulses are measured at end B, the first arrival time and the second arrival time of the PD pulses toward end B are denoted by t_{b1} and t_{b2},respectively. As a result, the calculated results X_A and X_B can be expressed as:

$$\begin{cases} X_A = L - \frac{1}{2}v(t_{a2} - t_{a1}) \\ X_B = L - \frac{1}{2}v(t_{b2} - t_{b1}) \end{cases} \tag{17}$$

Since the wave velocity will change with the transmission distance. Thus, if the change of wave velocity is not considered, the propagation velocity v' based on location results X_A and X_B in Eq. (18) can be derived from Eq. (17). However, if the change of the wave velocity is considered, Eq. (17) needs to be modified, that is, the value of wave velocity v' in X_A and X_B cannot be the same.

$$v' = \frac{2L - 2X_A}{t_{a2} - t_{a1}} \tag{18}$$

The PD source initiates an electrical pulse which is propagated simultaneously towards both ends of the cable. In other words, if the PD pulse is sent out at time T_0, the calculated location result X_A can be given by:

$$X_A = (t_{a1} - T_0)v' \tag{19}$$

However, because of the change of wave velocity, the time T_0 calculated at both ends are not the same in the improved single-terminal location method, in which can be expressed as T_{a0} toward end A and T_{b0} towards end B.

$$\begin{cases} T_{a0} = t_{a1} - \frac{X_A}{v'} \\ T_{b0} = t_{b1} - \frac{X_B}{v'} \end{cases} \tag{20}$$

Let $T_0 = (T_{a0} + T_{b0})/2$, the PD pulses generated from defect position are propagated towards both ends of the cable at time T_0. Thus, assuming that the PD pulses reaches end A and end B for the first time at time t_{a1} and t_{b1}, respectively, so that the wave velocities v_a and v_b can be expressed as:

$$\begin{cases} v_a = \frac{X_A}{t_{a1} - T_0} \\ v_b = \frac{X_B}{t_{b1} - T_0} \end{cases} \tag{21}$$

If the change of wave velocity is considered, the velocity v in Eq. (17) needs to be further modified, which the additional correction in two ends dv_a and dv_b can be given by:

$$\begin{cases} dv_a = v_a - \frac{v_a + v_b}{2} \\ dv_b = v_b - \frac{v_a + v_b}{2} \end{cases} \tag{22}$$

With the proposed location method, the first pulse which reaches the sensor is marked as the original pulse and the second pulse reaches the same sensor after reflecting from the far-end is marked as the reflected pulse. Thus, the arrival time difference Δt_a and Δt_b between the pulses can be determined as:

$$\begin{cases} \Delta t_a = t_{a2} - t_{a1} \\ \Delta t_b = t_{b2} - t_{b1} \end{cases} \tag{23}$$

Then, (17) can be eventually modified by:

$$\begin{cases} X_A = L - \frac{1}{2}(v + dv_a)\Delta t_a \\ X_B = L - \frac{1}{2}(v + dv_b)\Delta t_b \end{cases} \tag{24}$$

The threshold λ of value larger than zero represents the accuracy of the PD location algorithm. The following expression can be used to judge whether X_A and X_B satisfy (22).

$$|X_A + X_B - L| < \lambda \tag{25}$$

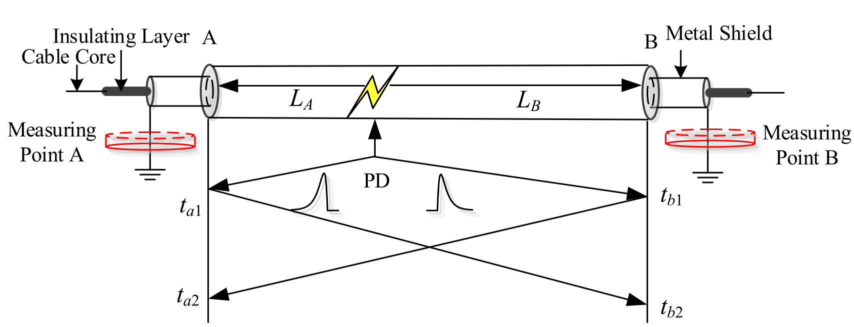

Fig. 3. Schematic diagram of PD location of cables based on improved single-terminal method.

The value of threshold λ is selected as required. If Eq. (25) does not hold, which means the further modification in Eq. (24) is needed. It can be seen that Eq. (24) consists of X_A and X_B, so they both need to be modified. Modifying the time differences Δt_a and Δt_b in Eq. (24) is equivalent to compensate the arrival time differences of end A and end B, where the compensations are denoted as dt_{a1} and dt_{b1}, respectively. The expression of dt_{a1} can be expressed as:

$$dt_{a1} = \frac{X_A + X_B - L}{100v} \tag{26}$$

Where v is the empirical estimation propagation velocity. dt_{b1} should satisfy the following relationship with dt_{a1}.

$$dt_{b1} = dt_{a1} * \frac{X_B}{X_A} = \frac{X_A + X_B - L}{100v} * \frac{X_B}{X_A} \tag{27}$$

Given $\Delta t_{a1} = \Delta t_a + dt_a$, $\Delta t_{b1} = \Delta t_b + dt_b$, substituting them into Eq. (24), then the modified PD location result X_{A1} and X_{B1} can be derived as:

$$\begin{cases} X_{A1} = L - \frac{1}{2}(v + dv_a)\Delta t_{a1} = L - \frac{1}{2}(v + dv_a)(\Delta t_a + dt_{a1}) \\ X_{B1} = L - \frac{1}{2}(v + dv_b)\Delta t_{b1} = L - \frac{1}{2}(v + dv_b)(\Delta t_b + dt_{b1}) \end{cases} \tag{28}$$

Compared with Eq. (24), it has:

$$|X_{A1} + X_{B1} - L| < |X_A + X_B - L| \tag{29}$$

Therefore, as illustrated in Eq. (29), it can be known that the modified PD source location results have a higher accuracy compared with the initial location results X_A and X_B.

In addition, substituting $X_A = X_{A1}$, $X_B = X_{B1}$ into Eq. (25) and evaluating whether the location results meet the requirements of location accuracy. If Eq. (25) holds, the modified X_A and X_B are location results of PD sources. Otherwise, further modification is needed, and the above steps are repeated until the requirements of location accuracy are satisfied.

In summary, the flowchart of the improved single-terminal PD location method based on time compensation is shown in Fig. 4.

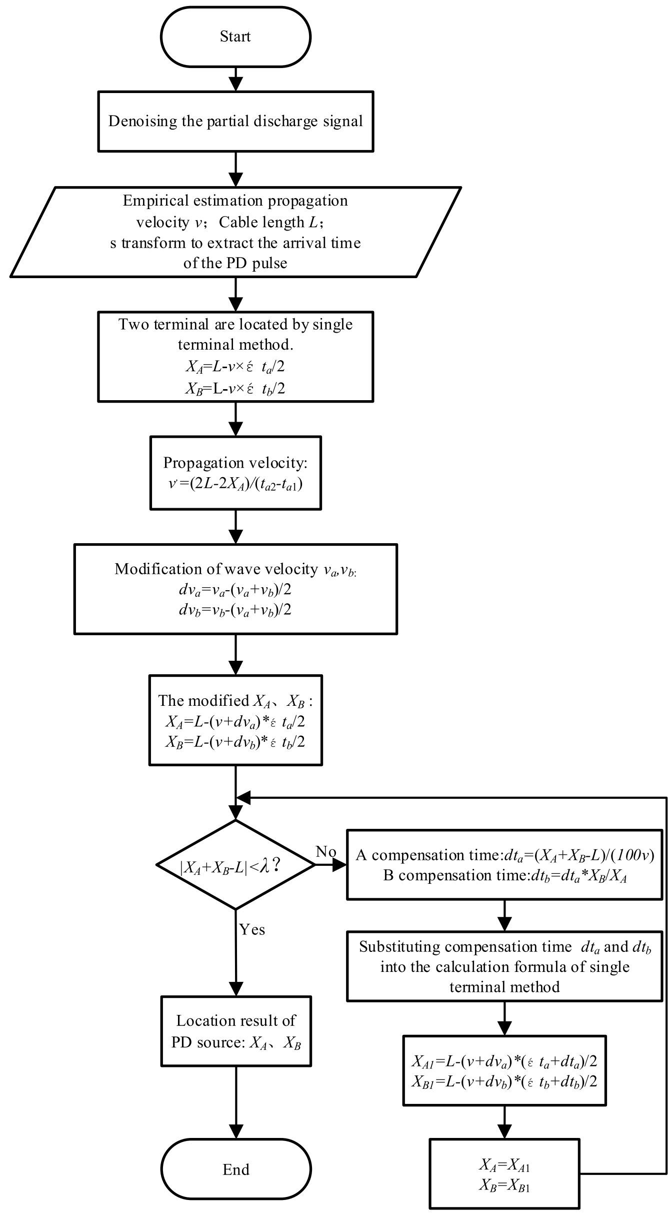

Fig. 4. Flowchart of the improved single-terminal PD location method.

4. Simulation results

4.1. Establishment of the simulation model

In order to verify the effectiveness of the proposed method, the experimental simulation model shown in Fig. 3 is established on PSCAD, the schematic of cable model is shown in Fig. 5 and the cable parameters are provided in Table 1. In the PD measuring system, the voltage level of the cable is 110 kV, the total length of the cable L is 1500 m. Let the distance between the PD pulse generated from the PD location and left end (end A) to 600 m and the right end (end B) to 900 m, that is, $L_A = 600$ m, $L_B = 900$ m. It has been proved that the PD pulse can be simulated by using the exponential decay oscillation model [11,16, 23-25]. Therefore, this paper uses a double exponential decay model to simulate PD signals for experiments, in which the sampling frequency is 100 MHz. The mathematical expression of the double exponential decay oscillation model can be expressed as:

$$s(t) = A\left(e^{-1.3t/\tau} - e^{-2.2t/\tau}\right)\sin(2\pi f_C t) \tag{30}$$

Where, the amplitude A is 20 mV, the attenuation constant τ is 1.5 μs, and the oscillation frequency f_C is 2 MHz.

To simulate the PD signal in the field, white Gaussian noise with a SNR of 2 db is added to the simulated signal. The PD signals of original signal and signal with noise are shown in Fig. 6.

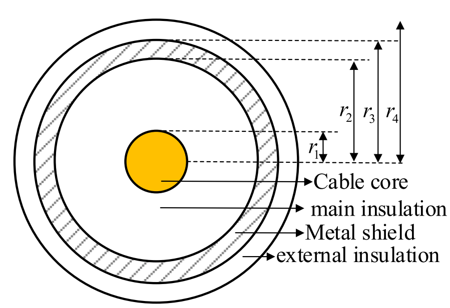

Fig. 5. Schematic of cable model.

4.2. Performance analysis of denoising method

As mentioned in Section 2, the PATEWT is adopted to denoise the above PD signals with Gaussian white noise. Thus, the denoising results can be shown in Fig. 7.

Table 1
Cable geometric parameters.

Parameter	Value
Cable core radius / mm	28.25
Internal insulation radius / mm	47.5
Metal shield radius / mm	50.9
external insulation Radius / mm	55.9
Shield resistivity /(Ω·m)	2.8 × 10–7
Cable core resistivity /(Ω·m)	1.75 × 10–8
Relative permittivity	2.3
Earth resistivity /(Ω·*m*)	100

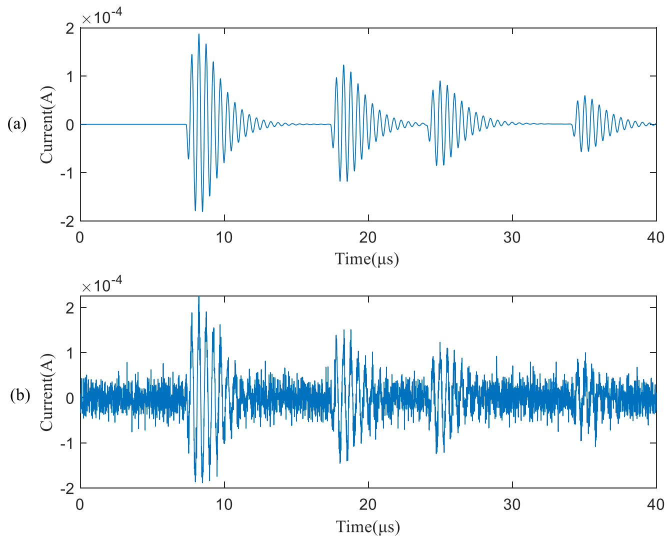

Fig. 6. (a) Simulated signal and (b) PD signal with noise.

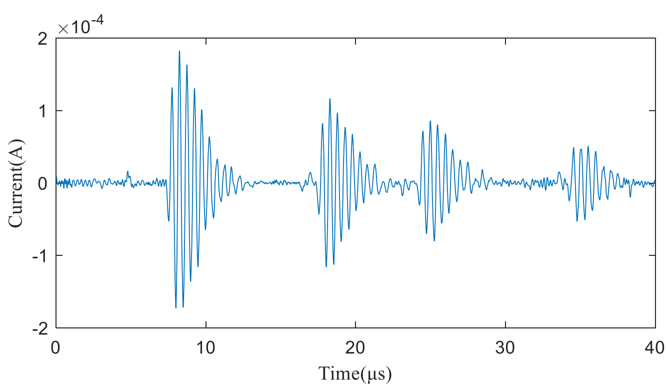

Fig. 7. Denoised PD signal by PATEWT denoising algorithm.

As shown in Fig. 7, the waveform of PD signal has a high identification degree after PATEWT denoising, which can guarantee the positioning accuracy of the location algorithm.

In order to verify the applicability of the PATEWT denoising algorithm, different levels of white Gaussian noise are added to the simulated PD signal. The proposed PATEWT, wavelet transform with soft threshold function (WT-STF), hard threshold function (WT-HTF), empirical wavelet transform with soft threshold function(EWT-STF) and hard threshold function (EWT-HTF) denoising methods are comparatively analyzed under the condition with a SNR of −5, −2, 0, 2, and 5 dB, respectively. In addition, in order to evaluate the denoising effect of the above methods, the normalized correlation coefficient (NCC), signal-to-noise ratio (SNR) and root mean square error (RMSE) are introduced as evaluation indicators. The comparison result with above assumption is shown in Fig. 8. Among them, the wavelet transform selects the db6 wavelet as a basis function, and the decomposition scale has 4 layers. The mathematical expressions of three indicators can be denoted as follows.

$$NCC = \frac{\sum_{t=1}^{N} Y(t)X(t)}{\sqrt{\sum_{t=1}^{N} Y^2(t) \sum_{t=1}^{N} X^2(t)}} \tag{31}$$

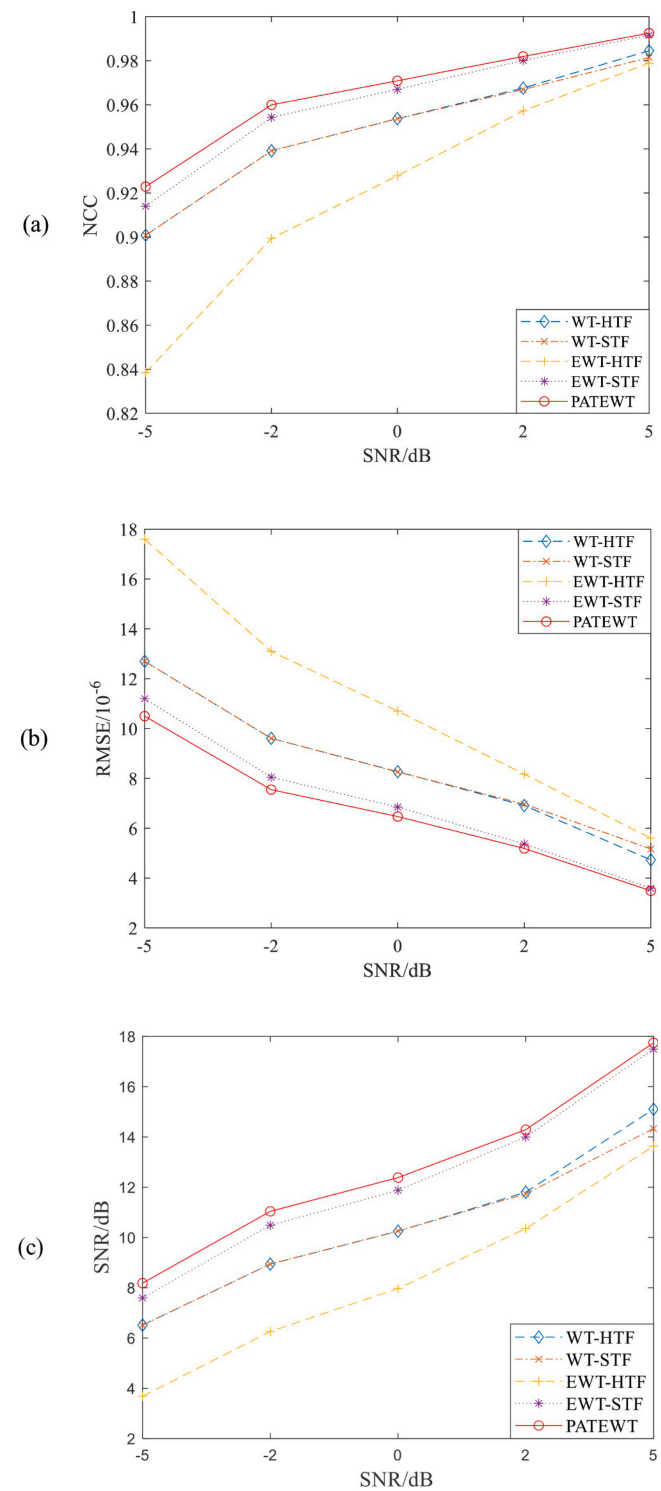

Fig. 8. Denoising results (a) NCC (b) RMSE (c) SNR under different SNR.

$$RMSE = \sqrt{\frac{1}{N}\sum_{t=1}^{N}(X(t) - Y(t))^2} \tag{32}$$

$$SNR = 101g\left(\frac{\sum_{t=1}^{N} Y^2(t)}{\sum_{t=1}^{N}(X(t) - Y(t))^2}\right) \tag{33}$$

where X(t) is the original signal, Y(t) is the signal after denoising.

As shown in Fig. 8, the denoising effect of EWT-STF is better than that of EWT-HTF and traditional wavelet transform for PD signals with different SNR noise. The adaptive threshold function proposed in this paper make the denoising effect further improved. Compared with the traditional wavelet denoising algorithm, the PATEWT denoising algorithm has an average increase of 0.02 in NCC, an average reduction of 2 × 10–6 in RMSE, and an average increase of 2db in SNR.

4.3. Analysis of the simulation result

The empirical estimation propagation velocity is set as $1.6*10^8$ m/s. Following the above location steps, the eventual denoising result is shown in Fig. 9.

In Fig. 9, there are a total of 6000 sampling points, the sampling frequency is 100 MHz, and the sampling time is 60 μs.Time axis from 1 to 6000 corresponds to 6000 sampling points, which also corresponds to time from 0 to 60 μs. Accordingly, frequency axis from 0 to 3000 corresponds to the frequency from 0 to $5*10^7$ Hz.

Due to only the arrival time of the first PD pulse and the second PD pulse need to be collected by S transform, so that the first two arrival time measured from end A are the 846th and the 1850th sampling point. Likewise, the first two arrival time measured from end B are the 1014th and the 1684th sampling point, i.e., the corresponding sampling time is: $t_{a1} = 8.46\ \mu s$, $t_{a2} = 18.50\ \mu s$, $t_{b1} = 10.14\ \mu s$, $t_{b2} = 16.84\ \mu s$, respectively.

The threshold λ is set as 0.01. Substituting $L = 1500$ m, $v = 1.6*10^8$ m/s, $t_{a1} = 8.46\ \mu s$, $t_{a2} = 18.50\ \mu s$, $t_{b1} = 10.14\ \mu s$, $t_{b2} = 16.84\ \mu s$ into formula Eq. (9) to Eq. (25). As a result, the proposed method locates the PD source 599.8 m away from end A.

Moreover, the location accuracy of the improved single-terminal method proposed in this paper is compared with traditional single-terminal method and the two-terminal method by setting different empirical estimation propagation velocity and selecting the PD source at different position. The comparison results are presented as follows:

Substituting $L = 1500$ m, $v = 1.6*10^8$ m/s and other measuring data when the length of L_A is taken as 200 m, 300 m, 400 m, 500 m, 600 m, 700 m and 750 m into formula Eq. (13) to Eq. (29). Thus, the location result is shown in Table 2. where, the δ represents the location error, and it can be expressed as:

$$\delta = \frac{|X_A - L_A|}{L} * 100\% \tag{30}$$

where X_A represents the distance calculated by the location algorithm, L_A represents the true distance, and L represents the full length of the cable.

It can be seen from Table 2, when the empirical estimation propagation velocity v is 1.6 × 10^8 m/s, location error of single-terminal method is always more than 5% and is larger than two-terminal method, However, when the actual distance of PD source is 200 m, location error of two-terminal method reached 4.03% and the error is quite large. When single-terminal method error of PD location is always controlled within 0.2%, the location accuracy is far higher than that of single-terminal and two-terminal methods.

In order to verify the effect of empirical estimation propagation velocity v on the proposed method, we change the value of v. In this way, the location result is shown in Tables 3 and 4, respectively.

It can be seen from Table 3, since the empirical estimated propagation velocity v is close to the actual propagation velocity, when $v = 1.8 \times 10^8$ m/s, the location errors of the single-terminal method, two-terminal method and improved single-terminal method are all within 0.5%. Among them, the maximum location error of the single-terminal method can reach 0.48%, and the robustness is poor. The location error of the two-terminal method and the improved single-terminal method can always be kept within 0.2%, so the robustness is good.

It can be seen from Table 4, when the empirical estimated propagation velocity v is 2.0 × 10^8 m / s, the PD location results are similar to those in Table 2. The accuracy of the improved single-terminal method is much higher than that of the single-terminal method and the two-terminal method, and its location error is always within 0.2%.

It can be known from Tables 2 to 4, when the empirical propagation velocity v takes different values, the error of the single-terminal or two-terminal location methods fluctuates greatly. However, the error of the improved single-terminal location method always keeps small, which is always stable within 0.2%. Therefore, compared with the other two traditional methods, the proposed method has a higher position accuracy and robustness.

5. Conclusions

According to the analysis and verification in this paper, the following conclusion can be obtained:

(1) In this paper, a PATEWT denoising algorithm is proposed. This algorithm is suitable for noisy PD signals with complex spectrum. It avoids the selection of wavelet base and decomposition scale by wavelet analysis algorithm. Meanwhile, it avoids selecting the number of decomposition modes artificially when the Fourier spectrum is divided by EWT based on extreme points.

(2) Compared with wavelet denoising and empirical wavelet denoising methods, the proposed PATEWT denoising method has

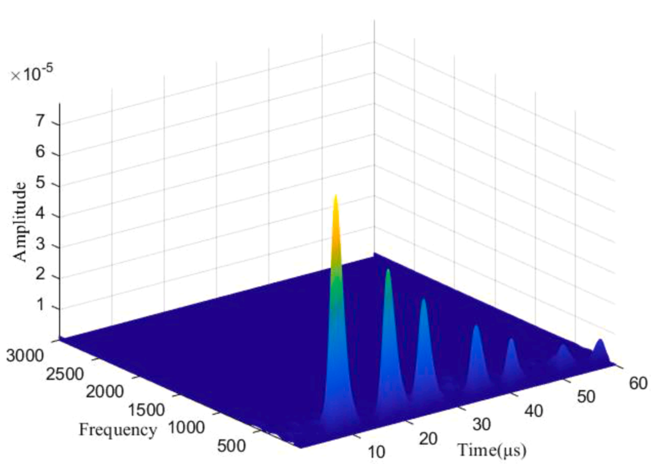

Fig. 9. PD signal with S transform.

Table 2
Location results when $v = 1.6 \times 10^8$ m/s.

True value L_A(m)	Two-terminal X_A(m)	δ/%	Single-terminal X_A(m)	δ/%	Improved single-terminal X_A(m)	δ/%
200	260.4	4.03	341.6	9.44	202.0	0.13
300	348.4	3.23	429.6	8.64	299.9	0.01
400	438.0	2.53	518.4	7.89	398.6	0.09
500	526.8	1.79	608.0	7.20	499.7	0.02
600	615.0	1.00	696.8	6.45	599.8	0.01
700	705.2	0.35	786.4	5.76	700.2	0.01
750	750.0	0.00	831.2	5.41	750.2	0.01

Table 3
Location results when $v = 1.8 \times 10^8$ m/s.

True value L_A(m)	Two-terminal X_A(m)	δ/%	Single-terminal X_A(m)	δ/%	Improved single-terminal X_A(m)	δ/%
200	199.2	0.05	192.8	0.48	202.8	0.19
300	298.2	0.12	295.8	0.28	300.1	0.01
400	399.0	0.07	395.7	0.29	398.3	0.11
500	498.9	0.07	496.5	0.23	499.6	0.03
600	598.8	0.08	596.4	0.24	599.9	0.01
700	699.6	0.03	697.2	0.19	700.1	0.01
750	750.0	0.00	747.6	0.16	750.2	0.01

Table 4
Location results when $v = 2.0 \times 10^8$ m/s.

True value L_A(m)	Two-terminal X_A(m)	δ/%	Single-terminal X_A(m)	δ/%	Improved single-terminal X_A(m)	δ/%
200	138.0	4.13	52.0	9.87	202.6	0.17
300	248.0	3.47	162.0	9.20	300.1	0.01
400	360.0	2.67	273.0	8.47	397.9	0.14
500	471.0	1.93	385.0	7.67	499.5	0.03
600	582.0	1.20	496.0	6.93	600.1	0.01
700	694.0	0.40	608.0	6.13	700.1	0.01
750	750.0	0.00	664.7	5.69	749.8	0.01

higher NCC, smaller MSE, and higher SNR. Moreover, the PD waveform after denoising is more conducive to subsequent analysis.

(3) This paper proposes an improved single-terminal PD location method based on time compensation as well. With this method, it eliminates the problem of large location error caused by the improper wave velocity of the PD signal in the traditional location methods, and avoids the synchronization problem existing in the two-terminal location method. In practice, the wave velocity will change with transmission distance, the method takes it into consideration to further improve the location accuracy.

(4) It is proved by simulation model that the proposed method has higher location accuracy and better robustness compared with the traditional single-terminal and two-terminal location methods even though the PD sources are at different positions.

In this paper, the proposed PD location method has high location accuracy for a single PD source. However, when there are multiple PD sources at the same time, the PD signals affect each other, so it is necessary to match and identify the PD signals first, and then locate the PD sources. In the follow-up study, we will study the location method when multiple PD sources exist simultaneously.

CRediT authorship contribution statement

Rui Liang: Software, Project administration. **Zhe Zhang:** Software, Data curation, Validation. **Hailong Li:** Software, Writing - original draft. **Peng Chi:** Conceptualization, Methodology, Validation. **Guoxin Li:** Supervision, Investigation. **Yunchun Tao:** Writing - review & editing.

Declaration of Competing Interest

The authors declare that they have no known competing financial interests or personal relationships that could have appeared to influence the work reported in this paper.

Acknowledgments

This research is supported by “The Fundamental Research Funds for the Central Universities” with No 2019GF06.

References

[1] F. Wen, L. Yuan, Wide area measurements based fault detection and location method for transmission lines, Prot. Control Mod. Power Syst. (2019) 53–64, https://doi.org/10.1186/s41601-019-0121-9. V(1).
[2] Nathalie Morette, Thierry Ditchi, Yacine Oussar, Feature extraction and ageing state recognition using partial discharges in cables under HVDC, Electr. Power Syst. Res. 178 (2020), 106053, https://doi.org/10.1016/j.epsr.2019.106053.
[3] C. Chen, K. Zhang, K. Yuan, et al., Novel detection scheme design considering cyber attacks on load frequency control[J], IEEE Trans. Industr. Inf. 14 (5) (2017) 1932–1941, https://doi.org/10.1109/TII.2017.2765313.
[4] Caio F.F.C. Cunha, André T. Carvalho, Mariane R. Petraglia, Antonio C.S. Lima, A new wavelet selection method for partial discharge denoising, Electr. Power Syst. Res. 125 (2015) 184–195, https://doi.org/10.1016/j.epsr.2015.04.005.
[5] Shimaa Barakat, Magdy B. Eteiba, Wael Ismael Wahba, Fault location in underground cables using ANFIS nets and discrete wavelet transform, J. Electr. Syst. Inf. Technol. 1 (3) (2014) 198–211, https://doi.org/10.1016/j.jesit.2014.12.003.
[6] C.K. Jung, J.B. Lee, X.H. Wang, Y.H. Song, Wavelet based noise cancellation technique for fault location on underground power cables, Electr. Power Syst. Res. 77 (2007) 1349–1362, https://doi.org/10.1016/j.epsr.2006.10.005.
[7] T.K. Abdel-Galil, A.H. El-Hag, A.M. Gaouda, et al., De-noising of partial discharge signal using eigen-decomposition technique, IEEE Trans. Dielectr. Electr. Insul. 15 (6) (2008) 1657–1662, https://doi.org/10.1109/TDEI.2008.4712670.
[8] M.B. Ashtiani, S.M. Shahrtash, Partial discharge de-noising employing adaptive singular value decomposition, IEEE Trans. Dielectr. Electr. Insul. 21 (2) (2014) 775–782, https://doi.org/10.1109/TDEI.2013.003894.
[9] M.S. Mashikian, R. Bansal, R.B. Northrop, Location and characterization of partial discharge sites in shielded power cables, IEEE Trans. Power Del. 5 (2) (1990) 833–839, https://doi.org/10.1109/61.53090.
[10] F.P. Mohamed, W.H. Siew, J.J. Soraghan, S.M. Strachan, J. McWilliam, Partial discharge location in power cables using a double ended method based on time triggering with GPS, IEEE Trans. Dielectr. Electr. Insul 20 (6) (2013) 2212–2221, https://doi.org/10.1109/TDEI.2013.6678872.
[11] S. Lan, Y. Hu, C. Kuo, Partial discharge location of power cables based on an improved phase difference method, IEEE Trans. Dielectr. Electr. Insul 26 (5) (2019) 1612–1619, https://doi.org/10.1109/TDEI.2019.008202.
[12] E.W. Shu, S. Boggs, Dispersion and PD detection in shielded power cable, IEEE Electr. Insul. Mag. 24 (1) (2008) 25–29, https://doi.org/10.1109/MEI.2008.4455500.
[13] E.W. Shu, S.A. Boggs, Effect of Dispersion on PD Pulse Propagation in Shielded Power Cable, in: 2008 Annual Report Conf on Electr Insul and Dielectric Phenomena, Quebec, QC, 2008, pp. 427–430, https://doi.org/10.1109/CEIDP.2008.4772878.
[14] G. Mugala, R. Eriksson, P. Pettersson, Dependence of XLPE insulated power cable wave propagation characteristics on design parameters, IEEE Trans. Dielectr. Electr. Insul 14 (2) (2007) 393–399, https://doi.org/10.1109/TDEI.2007.344619.
[15] R. MARDIANA, Q SU C, Partial discharge location in power cables using a phase difference method, IEEE Trans. Dielectr. Electr. Insul 17 (2010) 1738•1746, https://doi.org/10.1109/TDEI.2010.5658224.
[16] M. Xie, K. Zhou, S.L. Zhao, M. He, F.Z. Zhang, W. Zhao, Research on Partial Discharge Location Using Modified Cross-Correlation Method Considering Frequency Characteristic of Phase Velocity, Power Syst. Technol. 42 (5) (2018) 1661–1667, https://doi.org/10.13335/j.1000-3673.pst.2017.2390.
[17] J. GILLES, Empirical Wavelet Transform, IEEE Trans Signal Process. 61 (2013) 3999–4010, https://doi.org/10.1109/TSP.2013.2265222.
[18] M. Zhao, G. Xu, Feature extraction of power transformer vibration signals based on empirical wavelet transform and multiscale entropy, IET Sci. Meas. Technol. 12 (2018) 63–71, https://doi.org/10.1049/iet-smt.2017.0188.
[19] J. Gilles, K. Heal, A parameterless scale-space approach to find meaningful modes in histograms – Application to image and spectrum segmentation, Int. J. Wavelets Multiresolut. Inf. Process 2 (2014), https://doi.org/10.1142/S0219691314500441.
[20] C.L. Wang, C.L. Zhang, P.T. Zhang, Denoising algorithm based on wavelet adaptive threshold, Phys. Procedia 24 (2012) 678–685, https://doi.org/10.1016/j.phpro.2012.02.100.
[21] R. Arranz, A. Rodríguez, F. Muñoz, Detection of the natural frequency of transmission power lines applying S-transform on Transient Recovery Voltage, Electric Power Syst. Res. 182 (2020), 106142, https://doi.org/10.1016/j.epsr.2019.106142.
[22] X.Y. Zheng, M. Li Xiao, J.Y. Ding, Z.Y. Duan, Study on impedance traveling wave assemble algorithm in one terminal fault location system for transmission lines, in: 2008 Third International Conference on Electric Utility Deregulation and Restructuring and Power Technologies, 2008, pp. 1723–1726, https://doi.org/10.1109/DRPT.2008.4523684.

[23] Z.F. Du, P.K. Willett, M.S. Mashikian, Performance limits of PD location based on time-domain reflectometry, IEEE Trans. Dielectr. Electr. Insul. 4 (1997) 182–188, https://doi.org/10.1109/94.595245.
[24] X.J. Wang, M. Xie, Y.L.Huang K.Zhou, X.J. Rao, R. Li, Research on Partial Discharge Source Location for Power Cables Based on Time Reversal Phase Method, Power Syst. Technol. 44 (2020) 783–790, https://doi.org/10.13335/j.1000-3673.pst.2019.0434.
[25] B. Sheng, C.K. Zhou, D.M. Hepburn, X. Dong, G. Peers, Z. Zhou, Z. Tang, Partial discharge pulse propagation in power cable and partial discharge monitoring system, IEEE Trans. Dielectr. Electr. Insul. 21 (2014) 948–956, https://doi.org/10.1109/TDEI.2014.6832236.